The EMBO Journal (2011) 30, 3607–3619 | © 2011 European Molecular Biology Organization | Some Rights Reserved 0261-4189/11
www.embojournal.org

THE EMBO JOURNAL

EMBO open

The pore structure and gating mechanism of K2P channels

Paula L Piechotta[1,7], Markus Rapedius[2,7], Phillip J Stansfeld[3,7], Murali K Bollepalli[2,7], Gunter Erhlich[1], Isabelle Andres-Enguix[4], Hariolf Fritzenschaft[2], Niels Decher[5], Mark SP Sansom[3,6], Stephen J Tucker[4,6,*] and Thomas Baukrowitz[2,*]

[1]Universitätsklinikum Jena, Institute of Physiology II, Jena, Germany, [2]Institute of Physiology, Christian-Albrechts University, Kiel, Germany, [3]Structural and Computational Bioinformatics Unit, Department of Biochemistry, University of Oxford, Oxford, UK, [4]Department of Physics, Clarendon Laboratory, University of Oxford, Oxford, UK, [5]Institute of Physiology and Pathophysiology, University of Marburg, Marburg, Germany and [6]OXION Ion Channel Initiative, University of Oxford, Oxford, UK

Two-pore domain (K2P) potassium channels are important regulators of cellular electrical excitability. However, the structure of these channels and their gating mechanism, in particular the role of the bundle-crossing gate, are not well understood. Here, we report that quaternary ammonium (QA) ions bind with high-affinity deep within the pore of TREK-1 and have free access to their binding site before channel activation by intracellular pH or pressure. This demonstrates that, unlike most other K^+ channels, the bundle-crossing gate in this K2P channel is constitutively open. Furthermore, we used QA ions to probe the pore structure of TREK-1 by systematic scanning mutagenesis and comparison of these results with different possible structural models. This revealed that the TREK-1 pore most closely resembles the open-state structure of KvAP. We also found that mutations close to the selectivity filter and the nature of the permeant ion profoundly influence TREK-1 channel gating. These results demonstrate that the primary activation mechanisms in TREK-1 reside close to, or within the selectivity filter and do not involve gating at the cytoplasmic bundle crossing.

The EMBO Journal (2011) **30,** 3607–3619. doi:10.1038/emboj.2011.268; Published online 5 August 2011
Subject Categories: membranes & transport
Keywords: channel gating; K+ channel; K2P channel; potassium channel; TREK-1

*Corresponding authors. SJ Tucker, Department of Physics, Clarendon Laboratory, University of Oxford, Parks Road, Oxford OX1 3PU, UK. E-mail: stephen.tucker@physics.ox.ac.uk or T Baukrowitz, Institute of Physiology, Christian-Albrechts University, Kiel, Germany. E-mail: t.baukrowitz@physiologie.uni-kiel.de
[7]These authors contributed equally to this work

Received: 17 March 2011; accepted: 4 July 2011; published online: 5 August 2011

Introduction

Two-pore domain potassium (K2P) channels comprise a major and structurally distinct subset of the mammalian K^+ channel superfamily (Enyedi and Czirjak, 2010). The human genome contains 15 K2P channel genes (KCNK), which can be divided into six distinct subfamilies on the basis of both their structural and their functional properties, namely the TWIK, TASK, TREK, THIK, TALK and TRESK subfamilies. However, K2P channels differ to most other classes of K^+ channels because they assemble as a 'dimer of dimers' with each subunit containing four transmembrane segments (TM1–TM4); and thus, two of the four pore domains required to form a standard 'tetrameric' K^+ channel pore.

Functionally, K2P channels act as the classical background 'leak' potassium channels that contribute to the resting membrane potential in a wide variety of cells including neurons, skeletal and heart myocytes, glia and many different types of epithelial cells (Enyedi and Czirjak, 2010). Consequently, these channels exhibit one of the most versatile patterns of regulation known for any class of ion channel (Honore, 2007; Cohen *et al*, 2009; Mathie *et al*, 2010). One of the best known examples of such polymodal K2P channel regulation is the TREK-1 channel, which can be regulated by physical factors such as voltage, temperature and membrane stretch, as well as by a variety of chemical agents and natural ligands, including intracellular and extracellular protons, polyunsaturated fatty acids, phospholipids and volatile anaesthetics (Honore, 2007). Over the last decade, the physiological and pathophysiological importance of K2P channels has become increasingly clear and they now represent important potential therapeutic targets in cardiovascular disease, depression and memory disorders, as well as a variety of pain disorders and migraine (Heurteaux *et al*, 2006; Barel *et al*, 2008; Bayliss and Barrett, 2008; Lafreniere *et al*, 2010). However, in contrast to this rapidly increasing insight into their physiological role, the structural basis and molecular mechanisms of K2P channel gating and regulation are still very poorly understood (Cohen *et al*, 2008; Mathie *et al*, 2010).

In the other two major classes of K^+ channels, that is, the voltage-gated (Kv) and inwardly rectifying (Kir) channels, two structurally distinct gates have been proposed; a lower gate at the intracellular entrance of the pore (Yellen, 2002; Phillips and Nichols, 2003; Zhang *et al*, 2006), and an upper gate comprising the outer pore and the selectivity filter (Schulte *et al*, 2001; Yellen, 2002). The lower gate is thought to involve an aperture-like gating motion of the pore-lining inner transmembrane helices which constrict the permeation pathway at the helix bundle crossing (Swartz, 2004; Rapedius *et al*, 2007; Hibino *et al*, 2010). By contrast, the structural motions which control permeation at the upper gate are less well understood. Nevertheless, it appears that the two gates are tightly coupled and in many Kv channels opening of the lower gate triggers closure of the upper gate in a process

known as C-type inactivation (Yellen *et al*, 1994). Similar coupling has also been proposed for Kir channels (Schulte *et al*, 2001; Rapedius *et al*, 2007; Clarke *et al* 2010) and recent X-ray crystal structures of the KcsA channel in multiple different conformations suggest that subtle movements within the selectivity filter itself are responsible for this upper gating mechanism (Cuello *et al*, 2010a, b).

However, in K2P channels the relative importance of these two different gating mechanisms is currently unclear. Several studies have demonstrated a link between changes in extracellular pH and gating via the selectivity filter (Clarke *et al*, 2008; Cohen *et al*, 2008; Stansfeld *et al*, 2008; Sandoz *et al*, 2009; Niemeyer *et al*, 2010), but it is not fully understood how signals that operate through the intracellular C-terminal domain gate the K2P channel pore. For example, in TREK-1, the C-terminus is the primary sensor responsible for activation by membrane stretch, intracellular protons and lipids, and changes in the association of the C-terminus with the membrane are thought to underlie these gating processes (Honore, 2007). But whether these structural movements in the C-terminus activate the channel by opening the lower bundle-crossing gate, or whether they operate via the upper filter gate remains unclear (Cohen *et al*, 2009; Mathie *et al*, 2010).

In the Drosophila K2PØ channel, phosphorylation of the C-terminus has been demonstrated to result in structural changes in the outer pore (Zilberberg *et al*, 2001). But so far the status of the bundle-crossing gate in K2P channels has not been investigated directly, mainly due to a lack of high-affinity pore blockers that would be required to address such questions. Studies of TASK-3 channels have suggested that their response to voltage involves gating at the bundle crossing (Ashmole *et al*, 2009). Also, chimeric K2PØ/Kv channels have shown that the bundle crossing does indeed have the ability to act as a functional gate (Ben-Abu *et al*, 2009); however, only a single homotetrameric K2PØ pore domain was used in this study, and so whether this occurs in wild-type K2P channels is not known. Nevertheless, if K2P channels do possess a functional gate at the bundle crossing then regardless of whether there is an additional filter-gating mechanism, the bundle crossing must open in response to an activatory signal, otherwise the channels cannot become conductive.

In this study, we report that quaternary ammonium (QA) ions can act as high-affinity K2P channel pore blockers and we have used them to differentiate between a variety of different possible structural models of TREK-1. Importantly, we have also used them to demonstrate that the primary gating mechanism within TREK-1 exists close to, or within the selectivity filter and that unlike most other types of K^+ channels, gating of these channels does not involve opening and closure of the helix bundle crossing.

Results

QA ions are high-affinity intracellular pore blockers of K2P channels

QA ions have proven extremely valuable tools to study K^+ channels over the last 40 years, and although not all K^+ channels are blocked by extracellularly applied tetraethylammonium (TEA), most exhibit some degree of block by TEA when applied from the inside. In particular, it is this intracellular block by QA ions which has proven most useful as a probe of the inner pore structure and gating mechanism in many classes of K^+ channels (Armstrong, 1971; Baukrowitz and Yellen, 1996; Holmgren *et al*, 1997; Wilkens and Aldrich, 2006). However, because K2P channels are only poorly inhibited by extracellular TEA they have been traditionally labelled as 'TEA insensitive' (Lotshaw, 2007) and their response to intracellularly applied QA ions has largely been ignored.

We, therefore, explored the interaction of symmetrical QA ions with three different members of the K2P channel family; TREK-1, TASK-3 and TRESK. These K2P channels were chosen because they generated large currents (typically in the range of 2–40 nA) in giant inside-out patches excised from *Xenopus* oocytes, and are therefore particularly suitable to characterize intracellular blocker interactions and gating mechanisms. Surprisingly for a K^+ channel, we found that TREK-1 channels were remarkably insensitive to intracellular TEA with an IC_{50} value of $\sim$60 mM (Figure 1B and E). By contrast, TRESK channels and TASK-3 channels exhibited TEA sensitivities ($IC_{50} = 0.8 \pm 0.1$ and 3.3 ± 0.1 mM, respectively) similar to those seen in other classes of K^+ channels (Figure 1). Yet, despite this difference in TEA block, we found that increasing the length (i.e., hydrophobicity) of the alkyl chain in these symmetrical QA ions resulted in a remarkable increase in potency for all three K2P channels. Figure 1A shows the inhibition of TRESK channels exposed to various QA ions at a fixed concentration of 5 μM and Figure 1D the corresponding IC_{50} values obtained from detailed dose–response curves. The IC_{50} for QA inhibition for TRESK decreased sharply from TEA (0.8 ± 0.1 mM) to TButA (7 ± 1 μM) and to TPenA (0.3 ± 0.03 μM), plateaued for THexA (0.5 ± 0.04 μM) and THepA (0.5 ± 0.06 μM) and clearly increased again for TOctA (6 ± 1 μM).

In addition to this general increase in affinity with increasing chain length, the kinetics of TRESK inhibition also changed dramatically. For the smaller QA ions (TButA and TPenA), both the onset and recovery from inhibition were fairly rapid (Figure 1A). However, for THexA and THepA the recovery from inhibition was markedly slower than the onset, while for TOctA not only was the affinity reduced, but also both the onset and recovery from inhibition.

The other K2P channels, TREK-1 and TASK-3, also displayed a similar QA ion blocker profile as the TRESK channel (Figure 1E and F). However, for TASK-3 there was a larger increase in affinity from TPenA to THexA compared with TRESK channels. For TREK-1 channels, the chain length dependencies are shown in Figure 1B and E. However, it was difficult to obtain reliable dose–response curves for THepA and TOctA because these compounds produced a pronounced slow second component of inhibition at the concentrations required for inhibition of TREK-1. However, for THexA and smaller QA ions, inhibition could be determined reliably and in Figure 1C a typical dose–response curve for TPenA is shown.

QA inhibition in K2P channels closely resembles pore block in Kv channels

QA ions are known to inhibit both Kv channels and Kir channels from the intracellular side by binding to a site deep within the pore just below the selectivity filter. However, the biophysical properties of this block, such as

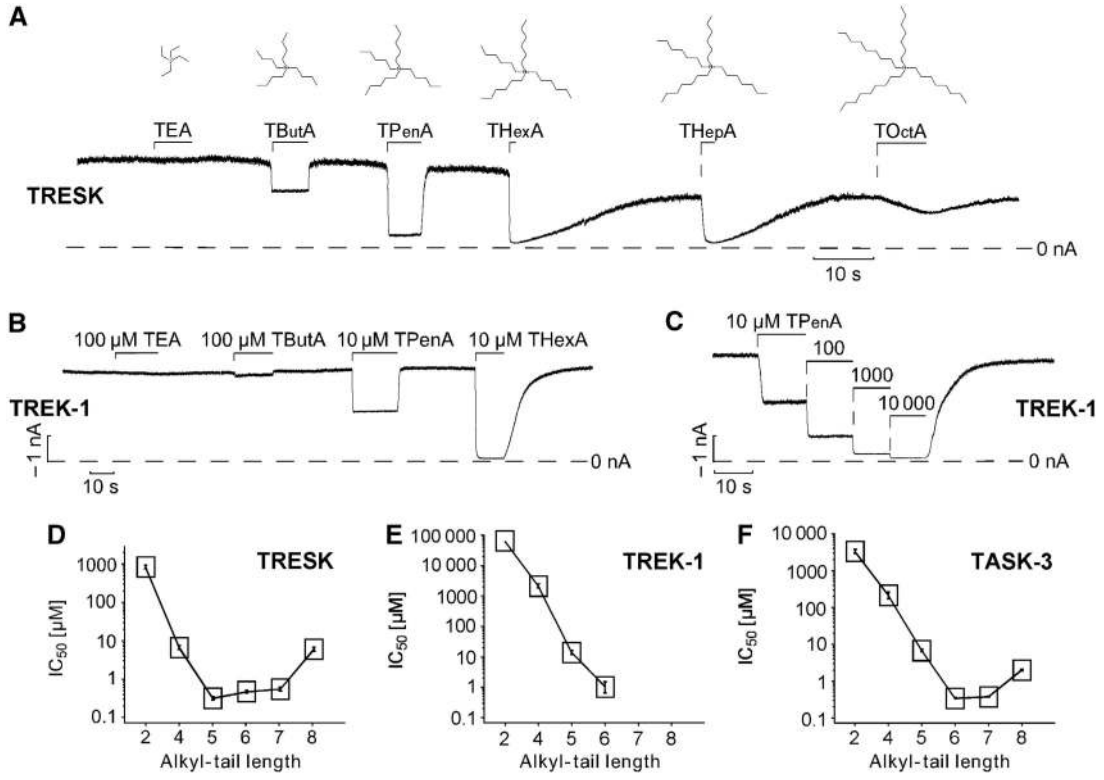

Figure 1 Quaternary ammonium (QA) ions are high-affinity inhibitors of K2P channels. (**A**) TRESK channel currents expressed in *Xenopus* oocytes measured at −80 mV in inside-out patches exposed to 5 μM of the indicated QA ions. (**B**) Application of 100 μM of TEA and TButA and 10 μM TPenA and THexA on TREK-1. (**C**) Representative current trace for determining the high-affinity block by TPenA in TREK-1. (**D**–**F**) Summary of IC_{50} values for current inhibition measured for TRESK ($n \geqslant 5$ experiments for each blocker), TREK-1 ($n \geqslant 4$ experiments for each blocker) and TASK-3 ($n \geqslant 3$ experiments for each blocker) channels determined for different chain length QA ions (note that for TREK-1, the IC_{50} for TEA was estimated due to insufficient block at very high concentrations).

voltage dependence and K^+ dependence, are quite distinct for these two classes of K^+ channels; for *Shaker* Kv channels, QA block of open channels exhibits relatively little dependence on voltage or extracellular [K^+] (Choi *et al*, 1993), whereas TPenA block of Kir1.1 is strongly voltage and $[K^+]_{ext}$ dependent (Oliver *et al*, 1998).

We, therefore, characterized the biophysical properties of QA block for K2P channels in direct comparison with the *Shaker* and Kir1.1 channels. We observed that TPenA block of TRESK displayed little voltage dependence (10% increase for a 100-mV voltage change); the current–voltage response was simply scaled down without affecting the weak but visible outward rectification (Figure 2A). This, therefore, closely resembles the type of pore block seen in Kv channels (Figure 2B), but is clearly distinct to the marked voltage-dependent block seen in Kir1.1 (Figure 2B). Similar results were also obtained for TREK-1 and TASK-3. We also observed that TPenA block of TRESK channels was only relatively weakly affected by the extracellular K^+ concentration, for example, the IC_{50} for TPenA reduced only 1.4-fold upon increasing extracellular K^+ from 4 to 120 mM. This is also similar to *Shaker* (2.1-fold), whereas in Kir1.1 TPenA inhibition decreased >10-fold upon raising extracellular K^+ (Figure 2C). Furthermore, the relationship between QA chain length and blocker potency for K2P channels showed greater similarity with *Shaker* than with Kir1.1 (Figure 2D). This remarkable similarity in the biophysical properties of QA block between K2P channels and the *Shaker* channel suggests that both channels share a similar blocking mechanism, and thus probably very similar pore structures.

Scoring of different TREK-1 models suggests QA ions bind to an 'open pore' structure

To identify the QA blocker binding site in TREK-1, we conducted systematic cysteine scanning mutagenesis of the inner pore (TM2 and TM4, and parts of P1 and P2) and examined the block by TPenA. Figure 3A demonstrates that mutation of either T157 in P1 or T266 in P2 results in a large reduction in the IC_{50} for TPenA block ($IC_{50} = 123 \pm 11$ and 102 ± 9 μM, respectively). These threonines are part of the highly conserved consensus K^+ channel filter motif (*T*XGYG), and a direct interaction of TPenA with these residues is consistent with the location of the TButA binding site identified in KcsA (PDB: 1J95). In that structure, TButA binds in an extended planar D_{2d} configuration deep within the inner pore cavity, just below the selectivity filter, and these highly conserved threonine residues form a critical interaction with the central nitrogen atom of the QA (Zhou *et al*, 2001). Furthermore, combining the T157C and L189C mutations produced an ~500-fold reduction in TPenA sensitivity (Figure 3B and C). These results suggest that the QA binding site in TREK-1 is likely to be in a similar position within the inner pore and that the data from Figure 3A could be used to distinguish between different possible structural models of the TREK-1 channel pore.

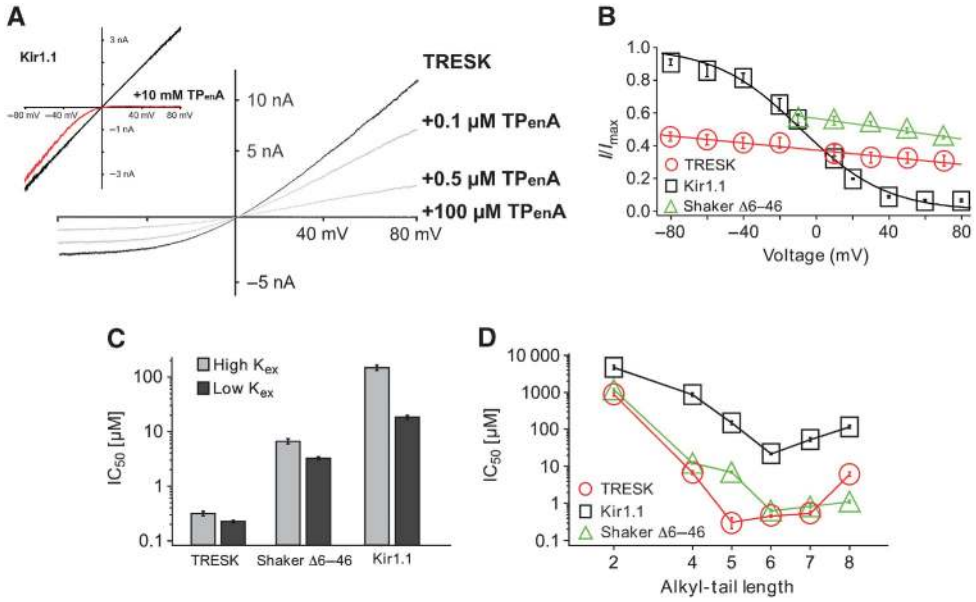

Figure 2 QA inhibition of K2P channels most closely resembles open-channel block in Kv channels. (**A**) Current–voltage relationship (ramp from −80 to +80 mV) in absence and presence of TPenA for TRESK and Kir1.1 channels at indicated concentrations. (**B**) Voltage dependence of inhibition measured at 0.3 µM, 2.5 mM and 5 µM TPenA for TRESK ($n=20$), Kir1.1 ($n=3$) and *Shaker*Δ6–46 (inactivation removed) ($n=11$), respectively. (**C**) IC_{50} of TPenA inhibition obtained at +40 mV for the indicated channels with high (120 mM) and low (4 mM) extracellular K^+ from at least four recordings of each channel and $[K^+]$ concentration. (**D**) Comparison of IC_{50} values obtained for different chain length QA ions in TRESK, Kir1.1 and *Shaker*Δ6–46 channels (at least $n=4$).

We, therefore, next created 18 different homology models based on the widest possible range of available structural templates; these included both open- and closed-state structures of channels such as KcsA, NaK, KvAP, MthK, MlotiK and Kv1.2. To quantify the interaction of TPenA with each of the different models, *in silico* docking was then performed; the nitrogen atom was positioned at the centre of the inner cavity, and TPenA aligned with the coordinate of the TButA molecule crystallized in the 1J95 KcsA crystal structure (Zhou *et al*, 2001). In each case, only the alkyl tails of TPenA were allowed to move and an optimal docking conformation for TPenA was established. Each model was then examined for the distance between the amino-acid side chains of the pore-lining helices and the optimally docked TPenA molecule. If this distance was ⩽4 Å for a specific residue and any part of the QA ion then it was scored as a 'hit', that is, likely to affect the interaction of TPenA with its binding site. The different models were then ranked according to whether this *in silico* analysis correlated with the effects of the *in vitro* functional mutagenesis. Our hypothesis was that the 'best fit' to the functional data would be provided by the most accurate structural model. We also included within this analysis several recently published structural models of the TREK-1 channel pore (Treptow and Klein, 2010; Milac *et al*, 2011). The results of this analysis are shown in Supplementary Table S1, and the best fit to the functional data is provided by a model based on the structure of KvAP (PDB: 1ORQ). This model identified five of the residues found in the cysteine scanning mutagenesis (Supplementary Table S1; Figure 3A), and most importantly generated no 'false positives', that is, residues predicted to interact with TPenA, but which show no functional difference in TPenA block when mutated.

The structure of this best-fit model of the TREK-1 pore is shown in Figure 4 along with TPenA docked into its predicted binding site (see also movie in Supplementary data). In addition to T157 and T266 in the selectivity filter, both I182 and L189 in TM2 interact directly with TPenA (Figure 4) and in TM4 a clear interaction with L304 is also seen. Although a number of residues identified in the functional mutagenesis scan (Figure 3) do not contribute to the predicted TPenA binding site in this particular model (Figure 4), they are not predicted to contribute to the binding site in any of the other models (Supplementary Table S1). Thus, their effects are either likely to be the result of an indirect influence on other residues which do form part of the binding site (e.g., P183C), or changes in the electrostatic profile of the inner pore (e.g., D309C). If these residues are excluded from the analysis, then the KvAP-based model accurately predicts five out of five possible residues within the binding site (T157, I182, L189, T266 and L304) and no false positives.

Interestingly, the KvAP-based structure is thought to be in an 'open' conformation, that is, it is open at the bundle crossing. Two other 'open-state' models based on MthK (3LDC) and Kv1.2 (2R9R) also allowed TPenA to dock in an extended planar conformation (Supplementary Figure S1). However, these models predict fewer positive interactions as well as including several false positives. In particular, interactions with F185 and F300 are predicted *in silico*; yet, no effect on TPenA block is seen upon functional mutagenesis of these residues (Supplementary Table S1; Supplementary Figure S1). By contrast, in all closed-state models, or those where the inner cavity is narrow, it was found that the alkyl tails of the docked TPenA adopt a more compressed (thus, less optimal) conformation in order to fit within the cavity (Supplementary Figure S2) and this finding is consistent with the poor fit of these models to our data. The recently published homology models of TREK-1 (Treptow and Klein, 2010; Milac *et al*, 2011) also score relatively low in our

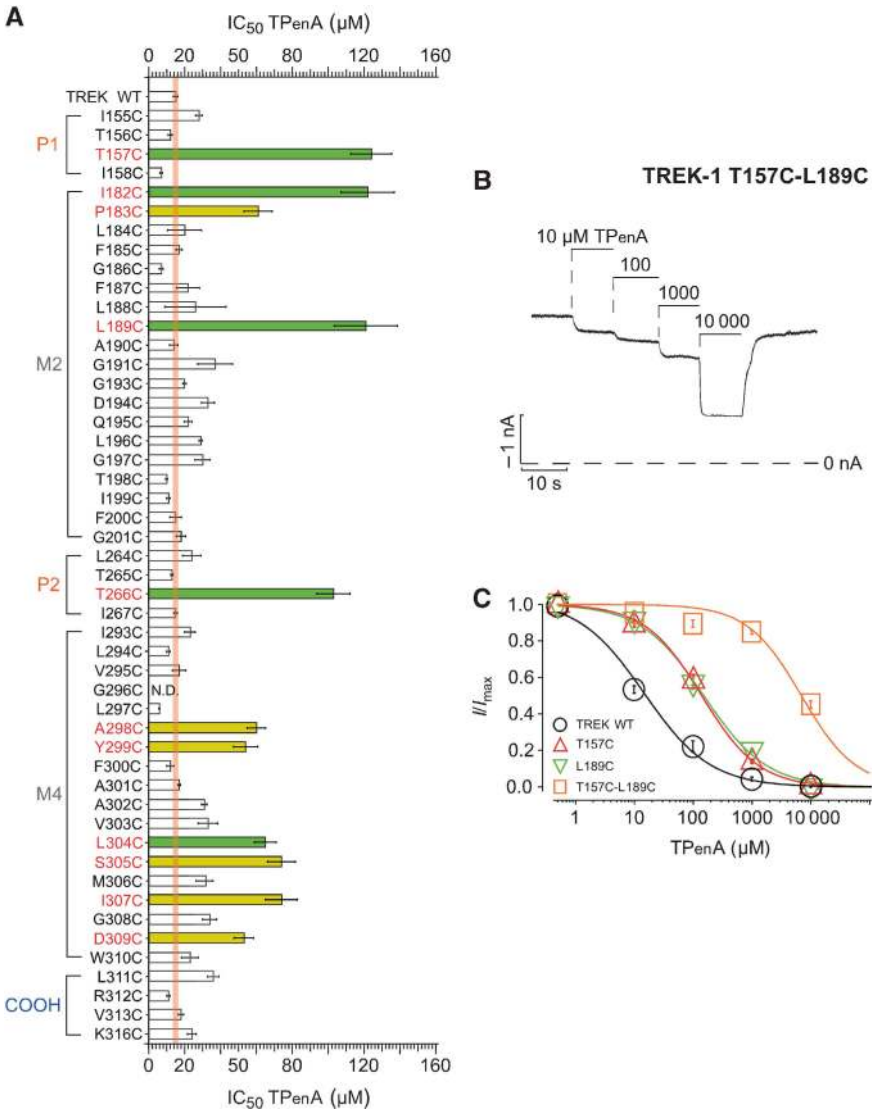

Figure 3 Identification of residues in the TREK-1 pore that affect TPenA block. (**A**) IC_{50} values of TPenA inhibition for TREK-1 WT ($n = 11$) channels and indicated mutations ($n \geqslant 4$). The orange line represents the deviation (s.e.m.) of the IC_{50} observed for WT channels. Green bars represent mutations thought to contribute directly to the QA binding site and in yellow those mutations which are not part of the binding site. (**B**) Current trace from the TREK T157C-L189C double mutation that results in a strongly decreased TPenA affinity. (**C**) Dose–response relationship from experiments such as in (**B**) fitted to a standard Hill equation for TREK WT, T157C and L189C mutations and the double mutant which dramatically reduces TPenA affinity; IC_{50} values of 13 ± 1, 123 ± 11, 120 ± 18 and 8149 ± 428 μM for WT ($n = 10$), T157C ($n = 5$), L189C ($n = 6$) and T157C-L189C ($n = 4$), respectively.

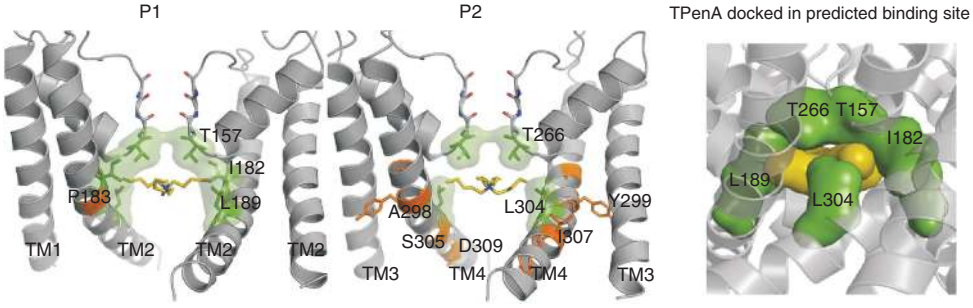

Figure 4 The QA ion binding site in TREK-1. TPenA is shown docked into the KvAP-based homology model of TREK-1. Two different side-view images are shown each with one pore-forming unit removed for clarity. The side chains of residues which affect TPenA inhibition are highlighted. Those predicted to directly interact with TPenA are show in green while those which do not appear to contribute directly to the binding site are shown in orange. The right hand panel shows a snapshot of the movie (Supplementary data), which shows a side view of how TPenA (yellow) docks well into the predicted binding site. Residues that affect TPenA block are shown in green. Coordinates for this model are provided in Supplementary data.

analysis, possibly because they mostly used KcsA as a starting structural template.

Alkyl chain length also affects the interaction of QA ions in silico

To further test the QA binding site in our best-fit model, we docked different sized QA molecules within the inner cavity to allow a qualitative comparison with the experimental obtained QA blocker affinities (Figure 1). In these unrestrained dockings, we observed that the nitrogen atom of the shorter chain QA ions (e.g., TEA and TButA) failed to locate accurately in a central position consistent with the low affinities in TREK-1. However, increasing the length of the alkyl chain located the QA ion to a more central position within the proposed binding site and allowed increasingly better interaction with the five identified TPenA interacting residues (Supplementary Figure S3). But, if the length of the alkyl chains was increased beyond seven carbons, then this resulted in a steric clash with the walls of the central cavity consistent with the observed drop in affinity for TOctA. Thus, these *in silico* results are in good overall agreement with our experimental data and support the accuracy of our KvAP-based TREK-1 model.

Exploiting the slow kinetics of THexA block

The structural similarities between the K2P and Kv channel pores, as well as their similarities in QA block raise the question whether K2P channels also use the bundle crossing as a gating mechanism. A well-established strategy to probe for a bundle-crossing gate in other K^+ channels has been to test whether pore blockers (e.g., QA ions) that have to pass through the bundle crossing to reach their binding site, can access this binding site when the channel is closed. A good example of this is the state-dependent inhibition of *Shaker* K^+ channels by large QA ions such as THexA. Figure 5A shows the activation of *Shaker* channels by a voltage jump from −80 to +40 mV in the presence of 20 μM THexA. The channels initially open to the same level as they do in the absence of THexA, but then exhibit a slow monoexponential current decay as they are blocked by THexA. This demonstrates that THexA only enters the pore *after* the bundle-crossing gate has been opened by voltage activation. However, to observe this time-dependent component of THexA pore block then channel opening must occur at a much faster rate than blocker binding.

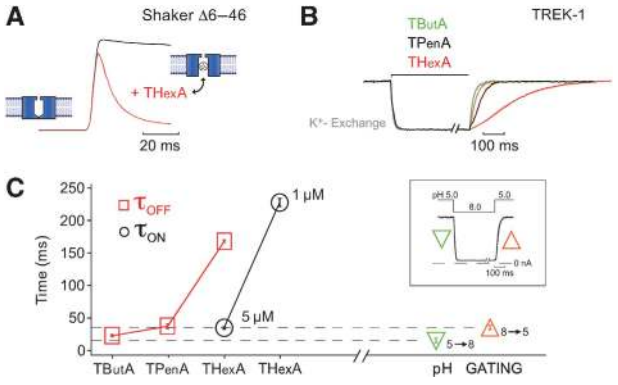

Figure 5 The slow kinetics of TREK-1 inhibition by THexA. (**A**) State-dependent inhibition of *Shaker*Δ6–46 channels with 20 μM THexA indicative of open-channel block. (**B**) Time course of TREK-1 inhibition of indicated QA compounds (5 μM THexA, 50 μM TPenA and 5 mM TButA) equalized for better comparison (i.e., 5 mM TButA produced only 60% inhibition) as monitored by a fast piezo-driven application system. (**C**) The blocking and unblocking time course from experiments as shown in (**B**) was fitted with a monoexponential function and τ values for QA inhibition (τ_{on}) and recovery from QA inhibition (τ_{off}) are plotted ($n \geqslant 3$ for each blocker). The dotted lines represent the time courses for activation/deactivation on pHi gating as illustrated in the inset ($n = 7$).

To apply this approach to K2P channel gating requires a very rapid activation mechanism and a pore blocker with slow binding kinetics. We, therefore, chose to exploit the activation of TREK-1 channels by low intracellular pH. Figure 5C (see also Figure 7A) shows that TREK-1 channels are completely closed at pH 8 and maximally activated at a pH of 5 with EC_{50} of 5.9 ± 0.1 and a Hill coefficient of 2.3 ± 0.1. Using a piezo-driven solution application system that allows rapid exchange of the intracellular solutions at the face of a giant inside-out patch within ~10 ms (Figure 5C, inset), we measured the speed of intracellular pH gating. We found that the kinetics of both pH activation (pH 8.0–5.0) and pH inhibition (pH 5.0–8.0) were very similar to the exchange of K^+/Na^+ (τ_{on} and τ_{off} in the range of 10–30 ms), indicating that pH gating must occur at the same rate (or faster than) the solution exchange (i.e., $\tau_{(pH\ 5=>8)} = 15.1 \pm 3.4$ ms and $\tau_{(pH\ 8=>5)} = 35.1 \pm 3.6$ ms).

Accordingly, any blocker used to probe the pH-gating mechanism should exhibit blocking and unblocking kinetics substantially slower than pH-gating kinetics. We, therefore, examined the kinetics of inhibition and recovery for TButA, TPenA and THexA. We found that the recovery of TREK currents from QA inhibition became progressively slower as the blocker chain length increased; for 5 μM THexA, the τ for channel unblocking was 167.7 ± 17 ms (Figure 5B and C), but the kinetics of THexA inhibition remained within the range of the solution exchange. However, reducing the concentration of THexA to 1 μM resulted in inhibition kinetics about sevenfold slower than the pH activation (Figure 5C). At this concentration (1 μM), the on and off rates were approximately equal and the steady-state current was inhibited by ~50%, consistent with a simple bimolecular reaction scheme for the blocker pore interaction.

QA block is not dependent on gating at the helix bundle crossing

We next examined the state dependence of THexA block for TREK-1 by exploiting the rapid kinetics of pHi gating and slow block by THexA. We found that when the channels were fully open at pH 5.0 and 1 μM THexA applied (i.e., the IC_{50} value), then the currents exhibited a slow time-dependent block to ~50% of the original current ($n = 5$, Figure 6A) and a similar slow recovery from inhibition. Likewise, when channels were activated by pH 5.0 with a solution containing 1 μM THexA, the current was activated to the same level as in the absence of THexA and subsequently declined to 50% of the peak current confirming that current activation (i.e., channel opening) precedes THexA block as pHi gating occurs at a much faster rate ($n = 6$, Figure 6B). However, when the blocker was applied before the activating pH jump, the current rapidly activated to ~50% of the control current without any indication of a slow-block component by THexA ($n = 6$, Figure 6C). This suggests that THexA has free access to its binding site while the channel is closed, and that the current activated by pH 5 is simply scaled down by the

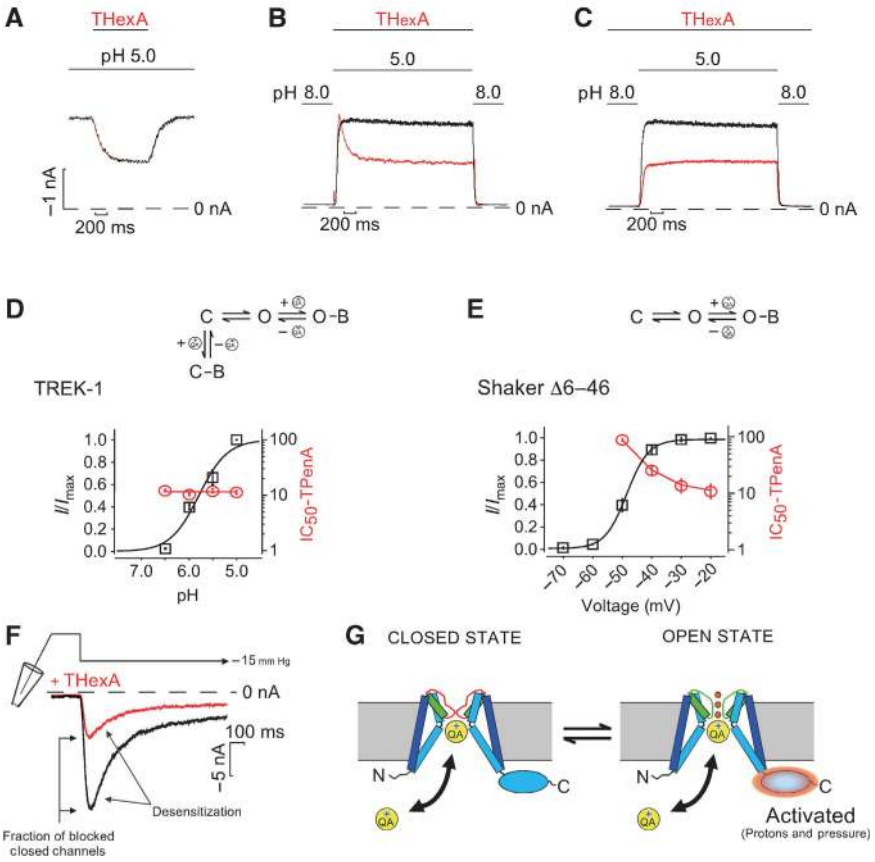

Figure 6 pH activation of TREK-1 does not involve the bundle crossing. (**A**) TREK currents activated by pH 5 during fast application and wash out of 1 μM THexA. (**B**) Closed channels at pH 8 were switched into a solution containing 1 μM THexA at pH 5 (red trace) and back to pH 8 showing fast pH-mediated opening and relatively slow blocking by THexA. (**C**) 1 μM THexA is continuously present during the switch from pH 8 to pH 5 (red trace) and the current is already pre-blocked to 50%, no slow block is observed. (**D**) As the Po for TREK-1 is increased by acidification to saturating levels no change in IC_{50} for TPenA inhibition is observed ($n \geqslant 6$ for each pH). (**E**) In contrast, in *Shaker*Δ6–46 channels the IC_{50} for TPenA inhibition decreases as relative current increases with voltage activation ($n \geqslant 4$ for each voltage). (**F**) Pressure activation by 15 mm Hg in absence (black trace) and presence of 1 μM THexA (red trace). (**G**) TREK-1-gating model. Large movements of the C-terminal regulatory domain are translated into small movements of TM helices to gate the channel at the filter and do not involve gating at the helix bundle crossing.

fraction of channels that have bound THexA in the closed state, that is, 50% at the IC_{50} concentration.

This result implies that THexA binds equally well to both the open and closed states of the channel and that consequently, the IC_{50} should be independent of the level of channel activation (i.e., the Po). TPenA inhibition of TREK-1 was, therefore, measured for pH values ranging from pH 7.0 to pH 5.0 and found to be identical despite the fact that the N*Po (i.e., activated current) increased >30-fold (Figure 6D). This is in clear contrast to *Shaker* K^+ channels where the IC_{50} for TPenA block decreases progressively as the fraction of open channel increases (Figure 6E). In *Shaker* channels this is what would be expected for a coupled equilibrium of closed channels that do not bind TPenA combined with open channels that do bind TPenA. By contrast, for TREK-1 channels, the closed-to-open state equilibrium does not affect the IC_{50} for TPenA inhibition because the blocker can bind to both states with similar affinity as illustrated by the model in Figure 6G.

Mechano-activation of TREK-1 does not involve gating at the bundle crossing

TREK-1 channels are also highly mechano-sensitive and exhibit a rapid activation in response to negative changes in pressure. If both pH and pressure open the same closed state, then we would predict that pressure activation also does not involve the helix bundle-crossing gate. However, we cannot exclude the possibility that TREK-1 might exist in two different closed states and that mechano-stimulation simply activates a different population of channels that might use the bundle-crossing gate. Therefore, we also tested the state dependence of THexA inhibition for TREK-1 activated by pressure. Figure 6F shows that a pressure jump from 0 to −15 mm Hg applied via the patch pipette rapidly activated TREK-1 channels followed by a phase desensitization, which reduced the current to 30% of the peak current as previously reported (Honore *et al*, 2006). Like pHi activation, this pressure activation occurred rapidly ($\tau = 25.5 \pm 2.5$ ms, $n = 3$) compared with block by THexA, and therefore allowed us to examine whether closed channels were already blocked by THexA before they were opened by pressure. As seen in Figure 6F, the pressure current evoked in the presence of 1 μM THexA was simply scaled down by $67 \pm 4.6\%$ ($n = 3$). This demonstrates that the blocker must have already bound to the closed TREK channels *before* they were activated by the rapid mechano-gating mechanism, otherwise the initial amplitude for pressure activation in the presence and absence would have been very similar. Thus, both the

pH- and pressure-gating mechanisms clearly do not involve a gated access to the pore via the cytoplasmic bundle crossing.

The selectivity filter directly influences TREK-1 channel gating

Together, the above results indicate that the entrance to the inner pore cavity is constitutively 'open' and thus permeable to K^+ ions even when TREK-1 channels are closed. Therefore, the principal activation gate must be located above the QA blocker binding site. An obvious location for this gate is the selectivity filter which is known to function as a gate in many other K^+ channels and which has also been proposed to contribute to the gating of K2P channels by extracellular pH (Cohen *et al*, 2008).

Our mutagenic scan of the TREK-1 pore in Figure 3A included a number of residues that are close to, or within, the highly conserved K^+ channel pore signature sequence; both ^{155}ITTI^{158} in P1 and ^{264}LTTI^{267} in P2 segments directly preceding the consensus GFG selectivity filter sequences. We, therefore, examined whether any of these mutations affect pHi gating, and found that four of these eight mutants caused a marked shift in the pH activation of TREK-1 (Figure 7). Mutation T157C in P1, as well as L264C and T266C in P2 decreased the $[H^+]$ required to half maximally activate the pH-sensitive fraction of the TREK-1 current (pH-$EC_{50} = -\log[H^+]$). Furthermore, these mutations also caused a significant fraction (1/3) of current to be active even at pH 8 producing a plateau in the pH range 8.0–7.5 (Supplementary Figure S5). By contrast, T156C and I158C in P1 and I267C in P2 all decreased the pH-EC_{50} (Figure 7C).

For those mutations that increased the pH-EC_{50}, a biphasic pH response was observed, that is, in addition to pH activation, a decrease in current was seen for pH values $\leqslant 6.0$ (Supplementary Figure S5). TREK-1 inhibition at low pH has been reported previously and is attributed to H^+ block of the pore that reduces the single channel conductance (Maingret *et al*, 1999). Consistent with this, H^+ inhibition would become more apparent for mutants with left shifted pH activation as seen in Figure 7B for T157C (see also Supplementary Figure S5).

The permeant ion directly affects TREK-1 pH gating

If, as these results suggest, the selectivity filter forms a structural part of the pHi-gating mechanism, then it should be intimately coupled to the mechanism of permeation and, thereby dependent on the nature of the permeant ion. We, therefore, examined the pH-EC_{50} for TREK-1 activation using K^+, Rb^+ or Tl^+ as the permeant ion ($[K^+]_i$ or $[Rb^+]_i$ or $[Tl^+]_I = 120$ mM; $[K^+]_{ex} = 4$ mM, at $+40$ mV). Figure 8A and B shows that when the permeant ion is changed from K^+ to Rb^+ at pH 8.0 that marked activation ($\sim$40% of the maximal current) is observed. Furthermore, at pH 6.0 the current is maximally activated. Thus, the sole replacement of K^+ by Rb^+ as the permeant ion caused a large change in $[H^+]$ required to activate TREK-1 (pH-EC_{50}-$Rb^+ \approx 8.0$ versus pH-EC_{50}-$K^+ = 5.8$). For Tl^+, the opposite is seen, namely a decrease of the pH-EC_{50} by $\sim$0.8 pH units.

These results support the concept that the selectivity filter is the gating structure in TREK-1 and that the intimate contact of the permeant ion with this gating structure directly determines the ligand-binding energy (i.e., the concentration of protons required) to open the gate. To rule out the possibility that the permeating ion species interferes with the bundle-crossing gating mechanism, we tested pHi gating in Kir1.1 channels. However, for Kir1.1, the permeant ion had no effect on the gating by pHi (Figure 8C and D). We also examined the effect of the permeant ion on QA inhibition and found no difference in the extent of TPenA inhibition with Rb^+ versus K^+ consistent with our principal conclusion that QA inhibits via direct pore block and not an indirect, allosteric effect on channel gating.

The intracellular pH gate differs from the extracellular pH gate

TREK-1 channels are also inhibited by low external pH. This inhibition is mediated by the protonation of histidines in the extracellular loop following TM1 and is thought to involve an inactivation mechanism analogous to the C-type inactivation seen in Kv channels (Cohen *et al*, 2008; Sandoz *et al*, 2009). External pH inhibition is markedly reduced by high external K^+ and enhanced by a mutation (S164Y) known to affect C-type inactivation (Cohen *et al*, 2008). Therefore, because both the intracellular and extracellular pH gates in TREK-1 appear to converge on the selectivity filter area, we examined whether they share any other similarities. However, no effect of external $[K^+]$ was observed on the gating of TREK-1 by intracellular pH. Also, the S164Y mutation did not alter the intracellular pH sensitivity (Figure 8E and F).

Discussion

In this study, we have identified QA ions as high-affinity K2P channel pore blockers which we have used to validate a

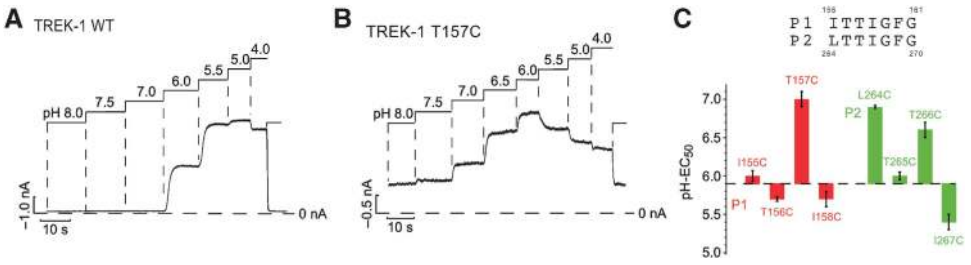

Figure 7 The selectivity filter is involved in pH gating of TREK-1. (**A**) Activation of TREK-1 channels by indicated intracellular pH, note the small blockage of the current by pH 4.0. (**B**) Similar experiment for the T157C mutant in P1. (**C**) Summary of the EC_{50} values for pH activation of mutations in P1/P2 region of TREK-1 compared with WT channels that is indicated by the dashed line (see Supplementary Figure S5).

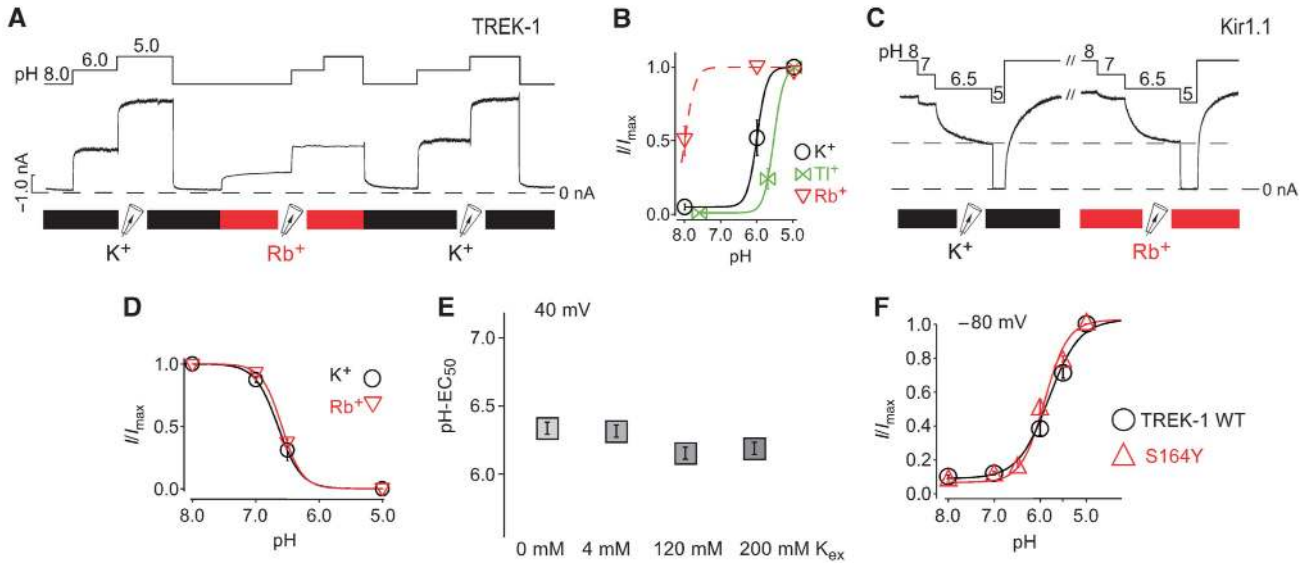

Figure 8 Effect of permeant ions on TREK-1 activation by pH. (**A**) pH activation of TREK-1 channels in the presence of Rb^+ in comparison with K^+ as permeating ion, measured at 40 mV. (**B**) Dose–response curves from experiments such as in (**A**) for different ionic species indicating a large effect of the permeant ion on pH activation in TREK-1 channels ($n \geqslant 4$ for each ion). (**C**) pH sensitivity of Kir1.1 in the presence of K^+ and Rb^+ as the conducting ion. (**D**) Dose–response curves from experiments such as in (**C**) fitted with standard Hill equation resulted in $pH_{0.5} = 6.62 \pm 0.068$ for K^+ ($n = 6$) and 6.58 ± 0.017 for Rb^+ ($n = 8$). (**E**) No effect of external $[K^+]$ concentration on the EC_{50} for pH activation in TREK-1 channels ($n \geqslant 6$ for each $[K^+]$ concentration). (**F**) Comparison of pH activation in TREK-1 WT ($EC_{50} = 5.9 \pm 0.1$; $n = 9$) versus S164Y mutant channels ($EC_{50} = 6.0 \pm 0.1$; $n = 6$) (a mutation related to extracellular pH sensitivity; Cohen *et al*, 2008) indicating no effect of this mutation on intracellular pH sensitivity.

structural model of the TREK-1 channel pore, and as a probe of the gating mechanism in these channels. Our results indicate that, unlike most other K^+ channels where the cytoplasmic bundle crossing has a dominant role in channel gating, TREK-1 channels exist primarily in an 'open-state' configuration and that the primary activation gate is located within, or close to, the selectivity filter.

Implications for K2P channel pharmacology

K2P channels are only poorly inhibited by classical K^+ channel blockers such as TEA, Cs^+ and 4-aminopyridine when applied from the extracellular site (Lotshaw, 2007). This atypical pharmacology has been attributed to the assumed asymmetric extracellular pore structure of these channels when compared with most other tetrameric K^+ channels. However, we report here that the intracellular pore of the K2P channels is blocked by QA ions in a very similar manner to the open pore block of Kv channels. This suggests that the structure of the inner cavity that interacts with QA ions is very similar in both types of channel. In Kv channels, this binding site is located deep within the inner pore cavity below the selectivity filter. Therefore, it will be interesting to examine whether any of the known Kv channel inhibitors that bind within the hydrophobic cavity also inhibit K2P channels.

The high-affinity K2P channel block seen with large QA ions (e.g., THexA) also suggests that these blockers could be valuable pharmacological tools to address the relative contribution of K2P and Kir channels to the resting membrane potential. Although Kir channels are also inhibited by QA ions (e.g., THexA), because of the steep voltage dependence of block (Figure 2A), inhibition at the resting membrane potential inhibition is negligible and thus a separation of the Kir and K2P conductances would be possible. The marked difference in K2P channel sensitivity to TEA (TREK-1 $IC_{50} \approx 60$ mM; TASK-3 3.3 ± 0.4 mM; TRESK 0.8 ± 0.1 mM) might also be exploited to distinguish between these subtypes in native preparations.

An open-state model of the TREK-1 channel pore

Employing systematic cysteine scanning mutagenesis of TM2, TM4 and parts of P1 and P2 we identified 12 mutants with markedly reduced TPenA sensitivity. This data set was used to score 18 different homology models of TREK-1 channel according to whether their side chains were in close proximity to a docked TPenA molecule. This method revealed KvAP to be the best structural template and identified a binding pocket for TPenA just below the selectivity filter that is made up of two threonines in P1 (T157) and P2 (T266) and three hydrophobic residues in TM2 and TM4 (I182, L189 and L304).

This comprehensive approach is in excellent agreement with a recent structural model of the TASK-1 pore, also based on KvAP, and which incorporated functional data for block by the TASK-1 subtype-specific blocker A1893 (Streit *et al*, 2011). Furthermore, our open-state model is also in good overall agreement with a structural model of the Drosophila K2PØ channel based on the crystal structure of Kv1.2 (Kollewe *et al*, 2009). Together, these studies provide strong evidence that the K2P channel pore shares extensive structural similarity with the open pore structure of Kv channels, and are also consistent with the principal finding of the blocker access studies, that is, that the bundle crossing is 'open', even when the channel is in its closed conformation.

Our analysis also indicates that, in the inner pore region at least, maintenance of a four-fold symmetry is critical, as was also seen in the models of K2PØ and TASK-3. The non-identical nature of the two-pore domains will obviously induce some degree of two-fold symmetry into the channel, but whether this extends beyond the non-identical nature of the side chains in the two pores is not clear, and is certainly not suggested by our model. However, our data only accurately distinguish between models in the pore cavity and do not differentiate between models, which propose different arrangements outside of this region.

The bundle-crossing gate in K2P channels

TREK channels possess one of the most versatile gating mechanisms known for any ion channel; mechanical stress, high temperature, negatively charged lipids, unsaturated fatty acids and low intracellular pH are all sensed by these channels and promote channel opening (Honore, 2007). In most K^+ channels, the primary gating mechanism involves an opening of the bundle crossing to permit the flow of ions across the membrane (Loussouarn *et al*, 2002; Yellen, 2002; Swartz, 2004). However, the location of this activation gate in TREK channels is so far unresolved.

In this study, we demonstrate that the bundle crossing is clearly open when TREK-1 channels are closed. To arrive at this conclusion, we took advantage of the very fast activation kinetics of TREK-1 (induced by either a rapid pH jump or a rapid pressure jump) and the slow blocking kinetics of THexA. These experiments demonstrate that the blocker has free access to its binding site in the closed state, and in particular, that the blocker affinity of closed and open TREK-1 channels is similar. This latter point is also supported by our finding that the IC_{50} for blocker inhibition is independent of the fraction of closed versus open TREK-1 channels (Figure 6D). The slow speed of the other activatory stimuli (e.g., arachidonic acid, anionic lipids or voltage activation) prevented us from directly probing for the status of the bundle-crossing gate. However, it seems likely that the closed state upon which all these activatory stimuli act is probably similar, and that they all act upon a channel where the bundle-crossing gate is constitutively open.

A selectivity filter gate in TREK-1

There is now strong evidence for the role of the selectivity filter in gating of many K^+ channels including Kv channels (Yellen, 2002), Kir channels (Schulte and Fakler, 2000) and KcsA channels (Cuello *et al*, 2010b). In those cases, however, the bundle crossing still operates as a functional gate and controls the status of the upper selectivity filter gate as seen in the open-state inactivation of, for example, *Shaker* K^+ channels (Yellen, 2002) and KcsA channels (Cuello *et al*, 2010a) or the closed-state inactivation of Kir1.1 channels (Rapedius *et al*, 2007). By contrast, our results suggest that the inner pore cavity of TREK-1 does not undergo any major structural changes upon channel activation and that the primary 'activation gate' appears to reside close to or within the selectivity filter. This gating behaviour most closely resembles CNG channels which are although thought to gate exclusively at the selectivity filter (Contreras and Holmgren, 2006; Contreras *et al*, 2008).

The following lines of evidence support the concept that the selectivity filter is the pH activation gate in TREK-1 channels. First, we found that the permeant ion has a major effect on pHi activation of TREK-1 as reflected in the profound difference in the $[H^+]$ required to activate TREK-1 channels in the order $Rb^+ > K^+ > Tl^+$ (Figure 8B). Substitution of K^+ by Rb^+ as the permeant ion appeared to stabilize the selectivity filter and, thus, making it more difficult to close the selectivity filter gate with a decreasing $[H^+]$. In contrast, Tl^+ will bind more weakly in the selectivity filter thereby making more it more easy to close the gate. These findings seamlessly join many studies on other K^+ channels that show a stabilization of the selectivity filter gate by Rb^+ (Demo and Yellen, 1992; Zhou and MacKinnon, 2003; Oliver *et al*, 2004; Cuello *et al*, 2010a) and a destabilization by Tl^+ (Lu *et al*, 2001; Zhou and MacKinnon, 2003; Oliver *et al*, 2004; Piskorowski and Aldrich, 2006; Schroeder and Hansen, 2008). By contrast, in Kir1.1 where the pHi gate is known to reside at the bundle crossing (Zhang *et al*, 2006; Rapedius *et al*, 2007), we found that the substitution of Rb^+ was without effect (Figure 8C and D). Second, several mutations of residues preceding the GFG motif in P1 and P2 profoundly alter pHi activation, some increased and other decreasing the EC_{50} for pHi activation. Further, the corresponding positions in P1 and P2 had very different effects on pHi gating, suggesting a functional asymmetry of the selectivity filter structure (Figure 7). Together, these results provide a convincing argument that the processes of gating and permeation are intimately coupled in TREK-1, and that the selectivity filter is not an isolated structural domain, but instead acts as the primary gating mechanism for activation in TREK-1 channels.

Despite the fact that they both appear to involve the selectivity filter, our results also suggest that gating by intracellular and extracellular pH may involve subtly different structural mechanisms. The S164Y mutation has a profound effect on pHo gating, but does not affect pHi gating. Also, pHi sensitivity is not dependent on extracellular $[K^+]$ (Figure 8E and F), whereas pHo gating is highly dependent (Cohen *et al*, 2008). It is possible that these gates converge upon different K^+ binding sites within the filter which might explain these differences, but clearly further studies will be required to address this.

Coupling of the C-terminus to the selectivity filter

We also demonstrate that the activation of TREK-1 by pressure does not involve opening of the channel at the helix bundle, and therefore most likely involves the same structural mechanism as pHi gating. Several previous studies have also indicated that these gating processes share a common mechanism because mutation of E321 in the intracellular C-terminus of TREK-1 dramatically affects both pHi gating and mechano-gating, and both processes are thought to involve changes in the interaction of the C-terminal domain with the membrane (Maingret *et al*, 1999; Honore *et al*, 2002; Chemin *et al*, 2005; Honore, 2007). Furthermore, activation by anionic lipids and polyunsaturated fatty acids such as arachidonic acid has been shown to involve the C-terminus (Honore, 2007). However, if the bundle crossing is not the gate, then the effect of these activatory signals must somehow be transduced upwards from the C-terminus through the TMs towards the selectivity filter. Thus, although our results demonstrate that the bundle crossing does not gate the channel, they do not imply that the TMs remain completely

rigid. We, therefore, propose that in order to transduce these gating signals to the filter gate, the TMs must still exhibit some degree of structural motion, even if it is quite subtle and does not constrict the bundle crossing.

Other types of K^+ channel have also been shown to exhibit structural coupling between the C-terminus and the selectivity filter (Clarke *et al* 2010; Cuello *et al*, 2010a, b), though whether similar movements occur in K2P channels are not clear. The unique structural asymmetry of the K2P channel pore suggests that the mechanisms involved in coupling may be fundamentally different and we speculate that TM4 is likely to have the dominant role in transduction of any gating signal because it is directly attached to the C-terminal regulatory domain. This, therefore, implies that there is a functional, as well as structural, asymmetry between TM2 and TM4 and it is tempting to speculate that the lack of functional gating at the bundle crossing in K2P channels may also be a reflection of this intrinsic structural asymmetry; all other K^+ channels which gate at the bundle crossing exhibit a four-fold symmetry, but in TREK-1 a preferential movement of TM4 induced by the C-terminal gating signal might have difficulty in producing effective opening and closure of the bundle crossing. However, gating at the selectivity filter probably only requires very small structural movements of the TM helices that do not need to be four-fold symmetrical.

In conclusion, our results demonstrate that the primary activation gating mechanism resides close to, or within the selectivity filter, and does not require opening and closure of the bundle crossing. These findings have major implications for our understanding of how K2P channels gate and the structural mechanisms which underlie their polymodal regulation.

Materials and methods

Mutagenesis, cRNA synthesis and oocytes injection

Rat TREK-1 (NM_172042), human TRESK, human TASK-3, rat Kir1.1 and the truncated version of *Shaker* channels (Shaker Δ6–46; N-type inactivation region (residues 6–46) removed) were used in this study. Site-directed mutagenesis was performed using the QuikChangeII system (Stratagene, La Jolla, CA, USA) and verified by sequencing. For oocyte expression, constructs were subcloned into the pBF expression vector. mRNAs were synthesized *in vitro* by using the SP6 mMESSAGE mMACHINE kit (Ambion, Austin, TX, USA) and stored in stock solutions at −80 °C. *Xenopus* oocytes were surgically removed from adult females and manually dissected. About 50 nl of a solution containing channel-specific mRNA was injected into Dumont stage VI oocytes. Oocytes were treated with 0.5 mg/ml collagenase type II (Sigma, Taufkirchen, Germany), defolliculated and incubated at 19°C for 1–3 days before use.

Electrophysiology

Giant patch recordings in inside-out configuration under voltage-clamp conditions were made at room temperature 1–7 days after mRNA injection. Pipettes were made from thick-walled borosilicate glass, had resistances of 0.3–0.9 MΩ (tip diameter of 5–15 μm) and filled with (in mM, pH adjusted to 7.2 with KOH; for TASK-3 measurements pH was adjusted to 9.0) 120 KCl, 10 HEPES and 1.8 $CaCl_2$. Low K^+ solution contained (in mM, pH adjusted to 7.2 with NaOH) 4 KCl, 116 mM NaCl, 10 HEPES and 1.8 $CaCl_2$. Currents were recorded with an EPC9 or EPC10 amplifier (HEKA electronics, Lamprecht, Germany) and sampled at 10 kHz with analogue filter set to 3 kHz (−3 dB). All solutions were applied to the cytoplasmic side of excised patches for the various ion channels via a multi-barrel pipette. For experiments on the pH gating or TAA^+-blocker kinetics, a fast-solution exchange system was used with double barrel theta-glass capillary attached to a piezo-driven device. The intracellular solution had the following composition in mM (K_{int}): 120 KCl, 10 HEPES, 2 K_2EGTA and 1 Na-Pyrophosphate, adjusted to the appropriate pH with HCl/KOH. Tetraethylammonium chloride (TEA), Tetrabutylammonium bromide (TButA), Tetrapentylammonium chloride (TPenA), Tetrahexylammonium chloride (THexA), Tetraheptylammonium bromide (THepA) and Tetraoctylammonium chloride (TOctA) were purchased from Sigma. All substances were stored as stocks (10–100 mM) at −20°C and diluted in K_{int} solution to final concentrations. All traces shown represent reversed inward currents recorded at a constant voltage of −80 mV (unless stated otherwise) under symmetrical K^+ concentrations. To study the pressure gating in TREK-1 channels, negative pressure was applied via the measuring pipette onto the extracellular side of the patch connected to a high-speed pressure clamp (HSPC-1) from Ala Scientific Instruments (Famingdale, NY, USA).

Data acquisition

Graphing was performed with Canvas Version 8 (Deneba Systems, USA) and statistical analysis was done with Microsoft Excel 2008 (Microsoft, USA). We used Igor Pro software (Wavemetrics Inc., USA) to analyse the data. The relative steady-state level of blockage for the different QA ions (at similar voltage) was fitted with the Hill equation:

$\text{Base} + (\text{max–base})/[1 + (x_{\text{half}}/x)^h]$, where Base = zero current, max = maximum current, x = ligand–concentration, x_{half} = value of concentration for half-maximal occupation of the ligand binding site (blockage by QA or activation by protons), rate = Hill coefficient. The values result from at least three experiments given as average ± standard error of the mean (s.e.m.). The same equation was used to describe the pH-dependent activation of TREK-1 currents. To obtain the level of zero current, we always applied 1 mM TPenA on pH-closed channels that was subtracted from all currents. For the fast-solution exchange experiments, the time course of Na^+/K^+ exchange, pH gating and QA blocking and unblocking was derived from a monoexponential fit.

Homology modelling

Homology models of rat TREK-1b were created using Modeller (9v8) (Sali and Blundell, 1993) based on KvAP (1ORQ), KcsA (1K4C, 3F5W, 3F7V, 3F7Y, 3FB5, 3FB6, 3FB8), MthK (3LDC), Kv1 (2R9R), MLotiK (3BEH) and NaK (2AHY, 3E86). The alignments of the pore regions used to create these models are shown in Supplementary Figure S4. Dockings of the QA ions were performed using Autodock version 4.2 (Goodsell *et al*, 1996). The QA ions were drawn using Marvin 5.3.4 (ChemAxon) and configured using Autodock Tools (Morris GM, J Comput Chem, 2009), which was also used to prepare the TREK-1 homology models for the docking runs. Initial dockings were performed using a grid of $30 \times 30 \times 30$ Å^3 that incorporated all residues in and around the central cavity of the homology models. The nitrogen atom of the QA ion was restrained at the centre of the central cavity, aligned with the coordinate of the TButA molecule crystallized in the 1J95 KcsA crystal structure (Zhou *et al*, 2001) and only the tails of the molecule were allowed to move. Coordinates for the best-fit model are shown in Supplementary data.

Supplementary data

Supplementary data are available at *The EMBO Journal* Online (http://www.embojournal.org).

Acknowledgements

This work was supported by research grants from the Deutsche Forschungsgemeinschaft (BA 1793/5-1), the Wellcome Trust and Pfizer UK.

Author contributions: SJT, TB, PLP, MR, MKB, ND, MSPS and PJS conceived and designed experiments. PLP, MR, PJS, MKB, IAE, HF and GE performed experiments. SJT, TB, PLP, MR, MKB, PJS, MSPS, IAE and GE analysed the data. SJT, MR and TB wrote the manuscript.

Conflict of interest

The authors declare that they have no conflict of interest.

References

Armstrong CM (1971) Interaction of tetraethylammonium ion derivatives with the potassium channels of giant axons. *J Gen Physiol* **58:** 413–437

Ashmole I, Vavoulis DV, Stansfeld PJ, Mehta PR, Feng JF, Sutcliffe MJ, Stanfield PR (2009) The response of the tandem pore potassium channel TASK-3 (K2P9.1) to voltage: gating at the cytoplasmic mouth. *J Physiol* **587**(Part 20)**:** 4769–4783

Barel O, Shalev SA, Ofir R, Cohen A, Zlotogora J, Shorer Z, Mazor G, Finer G, Khateeb S, Zilberberg N, Birk OS (2008) Maternally inherited Birk Barel mental retardation dysmorphism syndrome caused by a mutation in the genomically imprinted potassium channel KCNK9. *Am J Hum Genet* **83:** 193–199

Baukrowitz T, Yellen G (1996) Use-dependent blockers and exit rate of the last ion from the multi-ion pore of a K^+ channel. *Science* **271:** 653–656

Bayliss DA, Barrett PQ (2008) Emerging roles for two-pore-domain potassium channels and their potential therapeutic impact. *Trends Pharmacol Sci* **29:** 566–575

Ben-Abu Y, Zhou Y, Zilberberg N, Yifrach O (2009) Inverse coupling in leak and voltage-activated K^+ channel gates underlies distinct roles in electrical signaling. *Nat Struct Mol Biol* **16:** 71–79

Chemin J, Patel AJ, Duprat F, Lauritzen I, Lazdunski M, Honore E (2005) A phospholipid sensor controls mechanogating of the K^+ channel TREK-1. *EMBO J* **24:** 44–53

Choi KL, Mossman C, Aube J, Yellen G (1993) The internal quaternary ammonium receptor site of Shaker potassium channels. *Neuron* **10:** 533–541

Clarke CE, Veale EL, Wyse K, Vandenberg JI, Mathie A (2008) The M1P1 loop of TASK3 K2P channels apposes the selectivity filter and influences channel function. *J Biol Chem* **283:** 16985–16992

Clarke OB, Caputo AT, Hill AP, Vandenberg JI, Smith BJ, Gulbis JM (2010) Domain reorientation and rotation of an intracellular assembly regulate conduction in Kir potassium channels. *Cell* **141:** 1018–1029

Cohen A, Ben-Abu Y, Hen S, Zilberberg N (2008) A novel mechanism for human K2P2.1 channel gating. Facilitation of C-type gating by protonation of extracellular histidine residues. *J Biol Chem* **283:** 19448–19455

Cohen A, Ben-Abu Y, Zilberberg N (2009) Gating the pore of potassium leak channels. *Eur Biophys J* **39:** 61–73

Contreras JE, Holmgren M (2006) Access of quaternary ammonium blockers to the internal pore of cyclic nucleotide-gated channels: implications for the location of the gate. *J Gen Physiol* **127:** 481–494

Contreras JE, Srikumar D, Holmgren M (2008) Gating at the selectivity filter in cyclic nucleotide-gated channels. *Proc Natl Acad Sci U S A* **105:** 3310–3314

Cuello LG, Jogini V, Cortes DM, Pan AC, Gagnon DG, Dalmas O, Cordero-Morales JF, Chakrapani S, Roux B, Perozo E (2010a) Structural basis for the coupling between activation and inactivation gates in K^+ channels. *Nature* **466:** 272–275

Cuello LG, Jogini V, Cortes DM, Perozo E (2010b) Structural mechanism of C-type inactivation in K^+ channels. *Nature* **466:** 203–208

Demo SD, Yellen G (1992) Ion effects on gating of the Ca(2+)-activated K+ channel correlate with occupancy of the pore. *Biophys J* **61:** 639–648

Enyedi P, Czirjak G (2010) Molecular background of leak K+ currents: two-pore domain potassium channels. *Physiol Rev* **90:** 559–605

Goodsell DS, Morris GM, Olson AJ (1996) Automated docking of flexible ligands: applications of AutoDock. *J Mol Recognit* **9:** 1–5

Heurteaux C, Lucas G, Guy N, El Yacoubi M, Thummler S, Peng XD, Noble F, Blondeau N, Widmann C, Borsotto M, Gobbi G, Vaugeois JM, Debonnel G, Lazdunski M (2006) Deletion of the background potassium channel TREK-1 results in a depression-resistant phenotype. *Nat Neurosci* **9:** 1134–1141

Hibino H, Inanobe A, Furutani K, Murakami S, Findlay I, Kurachi Y (2010) Inwardly rectifying potassium channels: their structure, function, and physiological roles. *Physiol Rev* **90:** 291–366

Holmgren M, Smith PL, Yellen G (1997) Trapping of organic blockers by closing of voltage-dependent K+ channels: evidence for a trap door mechanism of activation gating. *J Gen Physiol* **109:** 527–535

Honore E (2007) The neuronal background K2P channels: focus on TREK1. *Nat Rev Neurosci* **8:** 251–261

Honore E, Maingret F, Lazdunski M, Patel AJ (2002) An intracellular proton sensor commands lipid- and mechano-gating of the K(+) channel TREK-1. *EMBO J* **21:** 2968–2976

Honore E, Patel AJ, Chemin J, Suchyna T, Sachs F (2006) Desensitization of mechano-gated K2P channels. *Proc Natl Acad Sci U S A* **103:** 6859–6864

Kollewe A, Lau AY, Sullivan A, Roux B, Goldstein SA (2009) A structural model for K2P potassium channels based on 23 pairs of interacting sites and continuum electrostatics. *J Gen Physiol* **134:** 53–68

Lafreniere RG, Cader MZ, Poulin JF, Andres-Enguix I, Simoneau M, Gupta N, Boisvert K, Lafreniere F, McLaughlan S, Dube MP, Marcinkiewicz MM, Ramagopalan S, Ansorge O, Brais B, Sequeiros J, Pereira-Monteiro JM, Griffiths LR, Tucker SJ, Ebers G, Rouleau GA (2010) A dominant-negative mutation in the TRESK potassium channel is linked to familial migraine with aura. *Nat Med* **16:** 1157–1160

Lotshaw DP (2007) Biophysical, pharmacological, and functional characteristics of cloned and native mammalian two-pore domain K+ channels. *Cell Biochem Biophys* **47:** 209–256

Loussouarn G, Rose T, Nichols CG (2002) Structural basis of inward rectifying potassium channel gating. *Trends Cardiovasc Med* **12:** 253–258

Lu T, Wu L, Xiao J, Yang J (2001) Permeant ion-dependent changes in gating of Kir2.1 inward rectifier potassium channels. *J Gen Physiol* **118:** 509–522

Maingret F, Patel AJ, Lesage F, Lazdunski M, Honore E (1999) Mechano- or acid stimulation, two interactive modes of activation of the TREK-1 potassium channel. *J Biol Chem* **274:** 26691–26696

Mathie A, Al-Moubarak E, Veale EL (2010) Gating of two pore domain potassium channels. *J Physiol* **588**(Part 17)**:** 3149–3156

Milac A, Anishkin A, Fatakia SN, Chow CC, Sukharev S, Guy HR (2011) Structural models of TREK channels and their gating mechanism. *Channels (Austin)* **5:** 23–33

Niemeyer MI, Cid LP, Pena-Munzenmayer G, Sepulveda FV (2010) Separate gating mechanisms mediate the regulation of K2P potassium channel TASK-2 by intra- and extracellular pH. *J Biol Chem* **285:** 16467–16475

Oliver D, Hahn H, Antz C, Ruppersberg JP, Fakler B (1998) Interaction of permeant and blocking ions in cloned inward-rectifier K^+ channels. *Biophys J* **74:** 2318–2326

Oliver D, Lien CC, Soom M, Baukrowitz T, Jonas P, Fakler B (2004) Functional conversion between A-type and delayed rectifier K^+ channels by membrane lipids. *Science* **304:** 265–270

Phillips LR, Nichols CG (2003) Ligand-induced closure of inward rectifier Kir6.2 channels traps spermine in the pore. *J Gen Physiol* **122:** 795–804

Piskorowski RA, Aldrich RW (2006) Relationship between pore occupancy and gating in BK potassium channels. *J Gen Physiol* **127:** 557–576

Rapedius M, Fowler PW, Shang L, Sansom MS, Tucker SJ, Baukrowitz T (2007) H bonding at the helix-bundle crossing controls gating in Kir potassium channels. *Neuron* **55:** 602–614

Sali A, Blundell TL (1993) Comparative protein modelling by satisfaction of spatial restraints. *J Mol Biol* **234:** 779–815

Sandoz G, Douguet D, Chatelain F, Lazdunski M, Lesage F (2009) Extracellular acidification exerts opposite actions on TREK1 and TREK2 potassium channels via a single conserved histidine residue. *Proc Natl Acad Sci U S A* **106:** 14628–14633

Schroeder I, Hansen UP (2008) Tl^+-induced micros gating of current indicates instability of the MaxiK selectivity filter as caused by ion/pore interaction. *J Gen Physiol* **131:** 365–378

Schulte U, Fakler B (2000) Gating of inward-rectifier K^+ channels by intracellular pH. *Eur J Biochem* **267:** 5837–5841

Schulte U, Weidemann S, Ludwig J, Ruppersberg J, Fakler B (2001) K^+-dependent gating of K(ir)1.1 channels is linked to pH gating through a conformational change in the pore. *J Physiol* **534**(Part 1)**:** 49–58

Stansfeld PJ, Grottesi A, Sands ZA, Sansom MS, Gedeck P, Gosling M, Cox B, Stanfield PR, Mitcheson JS, Sutcliffe MJ (2008) Insight into the mechanism of inactivation and pH sensitivity in potassium channels from molecular dynamics simulations. *Biochemistry* **47:** 7414–7422

Streit AK, Netter MF, Kempf F, Walecki M, Rinne S, Bollepalli MK, Preisig-Muller R, Renigunta V, Daut J, Baukrowitz T, Sansom M, Stansfeld PJ, Decher N (2011) A specific two-pore-domain potassium channel blocker defines the structure of the task-1 open pore. *J Biol Chem* **286:** 13977–13984

Swartz KJ (2004) Towards a structural view of gating in potassium channels. *Nat Rev Neurosci* **5:** 905–916

Treptow W, Klein ML (2010) The membrane-bound state of K2P potassium channels. *J Am Chem Soc* **132:** 8145–8151

Wilkens CM, Aldrich RW (2006) State-independent block of BK channels by an intracellular quaternary ammonium. *J Gen Physiol* **128:** 347–364

Yellen G (2002) The voltage-gated potassium channels and their relatives. *Nature* **419:** 35–42

Yellen G, Sodickson D, Chen TY, Jurman ME (1994) An engineered cysteine in the external mouth of a K+ channel allows inactivation to be modulated by metal binding. *Biophys J* **66:** 1068–1075

Zhang YY, Sackin H, Palmer LG (2006) Localization of the pH gate in Kir1.1 channels. *Biophys J* **91:** 2901–2909

Zhou M, Morais-Cabral JH, Mann S, MacKinnon R (2001) Potassium channel receptor site for the inactivation gate and quaternary amine inhibitors. *Nature* **411:** 657–661

Zhou Y, MacKinnon R (2003) The occupancy of ions in the K^+ selectivity filter: charge balance and coupling of ion binding to a protein conformational change underlie high conduction rates. *J Mol Biol* **333:** 965–975

Zilberberg N, Ilan N, Goldstein SA (2001) KCNKO: opening and closing the 2-P-domain potassium leak channel entails 'C-type' gating of the outer pore. *Neuron* **32:** 635–648